Electronic Supporting Information

Accessing water processable cyanido bridged chiral heterobimetallic Co(II)-Fe(III) one dimensional network

Anup Choudhury,[a] Céline Pichon,[b] Jean-Pascal Sutter,[b] Dobbidi Pamu,[c] Bipul Sarma,[a] Prashurya Pritam Mudoi[a] and Nayanmoni Gogoi*,[a]

[a] Department of Chemical Sciences, Tezpur University, Napaam-784028, Assam, India.

[b] Laboratoire de Chimie de Coordination du CNRS (LCC-CNRS), Université de Toulouse, CNRS, Toulouse, France

[c] Department of Physics, Indian Institute of Technology Guwahati, Guwahati 781039, India

List of Contents:

EXPERIMENTAL DETAILS:

Materials and methods:

Chemicals were purchased from Merck India, TCI chemicals and Sigma Aldrich India and used without further purification. Solvents were procured from Merck India and Rankem India and were distilled prior to use, using common purification techniques. Melting points were collected on a Buchi M-560 Melting Point apparatus and are reported uncorrected. Elemental analyses were performed using Perkin Elmer PR-2400 Series II CHNO/S analyzer. Perkin Elmer Frontier MIR-FIR FT-IR spectrophotometer is used to obtain Fourier-transformed infrared spectra from 400 to 4000 cm^{-1} using KBr diluted discs. A Shimadzu UV-visible 2550 spectrophotometer was used to record the UV-visible spectra. Solid state UV-visible spectra were recorded on a Shimadzu 2450 spectrophotometer.^{1}H-NMR spectra are recorded on a JEOL JNM-ECS 400 NMR spectrometer at 400 MHz with TMS as the internal standard. The solvent used for ^{1}H-NMR and ^{13}C-NMR was DMSO-d$_6$ and the obtained data are expressed in delta (∂) parts per million. Powder X-ray diffraction pattern were recorded on a Rigaku Multiflex instrument using a Nickel filtered Cu-Kα (0.15418 nm) radiation source and scintillation counter detector. Atomic absorption spectroscopic studies were performed using AAS-ICE-3500 atomic absorption spectroscopy analyzer. Thermogravimetric analyses were performed with the help of Thermal Analyzer (Model TGA-50 and DSC-60, Schimadzu). ESI-MS analyses were recorded using a Q-Tof Premier Waters analyzer. LC-mass spectrum was recorded using a Waters Q-Tof premier analyzer. MALDI-TOF MS analysis was carried out using a Bruker Autoflex Speed analyzer. Dynamic light scattering measurements were performed on a Litesizer 500-82649104-BM10 analyzer.

Crystallography: Single crystals of all the compounds suitable for diffraction measurements were used directly from the reaction mixtures. The diffraction data for the compounds were collected on a Bruker APEX-II CCD Diffractometer using MoKα radiation (λ=0.71073 Å) using φ and ω scans of narrow (0.5°) frames at 100 K. All the structures were solved by direct methods using SHELXL-97 as implemented in the WinGX program system.[1] Anisotropic refinement was executed on all non-hydrogen atoms. The aliphatic and aromatic hydrogen atoms were placed on calculated positions but were allowed to ride on their parent atoms during subsequent cycles of refinements. Positions of N-H and O-H hydrogen atoms could not be on the located on the Fourier map due to presence of heavy metal atoms and N-H hydrogens were fixed at the calculated positions.

Electrical measurements: Polarization measurements were performed on pellet of powder samples at room temperature using a Radiant Precision-609B ferroelectric tester. Crystals of compound **1** were grinded to make powder and the powder was mixed with polyvinyl alcohol (PVA) and pressed into circular pellets of diameter 10 mm and thickness 1 mm under an isostatic pressure of 5×10^6 Nm^{-2} using a hydraulic press. Crystals of compounds **2** were grinded to make powder and the powder was pressed into circular pellets of diameter 12 mm and thickness 1.56 mm under an isostatic pressure of 5×10^6 Nm^{-2} using a hydraulic press. High purity silver conducting paste was used to coat on the pellets for better electrical contact during P-E measurements. After performing the P-E measurement for the solid sample of **2**, the silver coated pellet was dissolved in minimum volume of distilled water, immediately filtered through suction and the water was removed under vacuum at a temperature *ca.* 40 °C. The solid obtained was washed with methanol followed by diethyl ether and dried over silica in desiccator. Silver coated pellet was prepared with diameter 10 mm and thickness 1.50 mm for the solid recovered from water (**2′**).

Magnetic Measurements: Magnetic measurements were carried out with a Quantum Design MPMS 5S SQUID magnetometer in the temperature range 2−300 K. The measurements were performed a polycrystalline sample. The powder was mixed with grease and put in gelatin capsules. The temperature dependences of the magnetization were measured in an applied field of 1kOe and the isothermal field dependence of the magnetizations were collected up to 5 T. The molar susceptibility (χ_M) was corrected for sample holder, grease and for the diamagnetic contribution of all the atoms by using Pascal's tables. AC susceptibility has been collected in zero field and with applied field. All results are plotted for a [CoFe] unit. The temperature dependence of the magnetic susceptibility of **2** was analyzed with the expression for an Heisenberg chain of classical spins[2] given below:

$$x_M = \frac{N\mu_B^2}{6k_BT}\left[(M_{Fe} + M_{Co})^2\frac{1+u}{1-u} + (M_{Fe} - M_{Co})^2\frac{1-u}{1+u}\right]$$

where $M_a = g_a\sqrt{S_a(S_a+1)}$, a = Fe, Co

$$u = coth(J^e/kT) - kT/J^e$$

$$J^e = J\sqrt{S_{Fe}(S_{Fe}+1)S_{Co}(S_{Co}+1)}$$

Synthesis of (l)-2-hydroxypropanehydrazide: The chiral hydrazide is prepared by following a reported synthetic procedure.[3] Equimolar amounts of methyl-*l*(-)-lactate (5 g, 48.025 mmol) and hydrazine monohydrate (1.5 mL, 48.025 mmol) were mixed and the mixture was allowed to reflux for 6 hours. Methanol and water produced in the reaction were removed under reduced pressure. The final colourless oil was used for further synthesis. Yield: 4.4 g (88%). IR (KBr): υ/cm^{-1} = 3437 (br), 1649 (m), 1452(w), 1373 (w), 1123 (w), 1045 (m), 992 (w), 930 (w), 874 (w). ^{1}H NMR (δ, ppm, DMSO-d_6): 8.8 (br, 1H), 3.9 (q, J = 7.0 Hz, 1H), 1.1 (d, J = 7.0, 3H). ^{13}C NMR (δ, ppm, DMSO-d_6): 174.1 (C=O), 67.1 (CHOH) and 21.3 (CH_3).

Synthesis of 2,6-diacetylpyridine bis(l-lactic acid hydrazide)(*l*-daplh):2,6-diacetylpyridine (1.632 g, 10.0 mmol) and *l*-lactic acid hydrazide (2.082 g, 20.0 mmol) were dissolved in 40 mL ethanol and one drop of hydrochloric acid was added. The resulting solution was heated to reflux and stirred. After about ten minutes a yellow solid began forming. Reflux was continued for another one hour. The mixture was cooled to room temperature and the solid formed was filtered, washed with ethanol and dried. Yield: 3.052 g(91%); M. p.: 187-190°C. IR (KBr): υ/cm^{-1} = 3338 (br), 2998 (w), 2981 (w), 2927 (w), 1668 (s), 1571 (w), 1523 (m), 1453 (m), 1365 (w), 1126 (s), 988 (w), 814 (m), 631 (m), 527 (w). Elemental analysis: Found (calculated for $C_{15}H_{21}N_5O_4$): C, 53.21(53.72); H,6.17(6.31); N,20.34(20.88).

Synthesis of [Co(l-daplh)(H$_2$O)$_2$](NO$_3$)$_2$·2H$_2$O (**1**): *l*-daplh (1.19 mmol, 0.400 g) was suspended in 20 mL ethanol and heated to 55°C.$Co(NO_3)_2\cdot6H_2O$ (1.19 mmol, 0.346 g) was dissolved in 20 mL of ethanol and was added to the ligand suspension. Immediate dissolution of the ligand was observed. The mixture was refluxed for one hour. A clear dark red solution resulted which was cooled to room temperature and filtered. Slow evaporation of the filtrate gave orange-red crystals of [Co(l-daplh)(H_2O)$_2$](NO_3)$_2\cdot$2H_2O after 14 days. The mother liquor was decanted and crystals were washed with minimum amount of ethanol and then dried with diethyl ether. Yield: 0.584 g (83%, based on Co). M. p.: >250 °C.IR (KBr): υ/cm^{-1}= 3411 (br), 1641 (s), 1533 (m), 1384 (s), 1273 (w), 1225 (w), 1208 (w), 1176 (w), 1055 (w), 1017 (w), 892 (w), 816 (w), 763 (w), 619 (w). Elemental analysis: Found (calculated for $CoC_{15}H_{29}N_7O_{14}$): C,30.36(30.52); H,4.61(4.95); N,16.53(16.61).

*Synthesis of [{K(H$_2$O)$_2$}{K(H$_2$O)}{Co(l-daplh)}$_2${Fe(CN)$_6$}$_2$]$_n$ (**2**):* To a solution of [Co(*l*-daplh)(H_2O)$_2$](NO_3)$_2\cdot$2H_2O(0.036 mmol, 0.020 g) in 5 mL methanol, KSCN (0.18 mmol, 0.018 g) was added. The reaction mixture was stirred at room temperature for 1 hour. The solution was then filtered and filtrate was layered with a solution of $K_3[Fe(CN)_6]$ (0.036 mmol, 0.0112 g) in 1 mL distilled water using water : methanol (1:1) as buffer. The layered solution was kept undisturbed in dark. Dark brown needle-shaped crystals of **2** were obtained after one week. The mother liquor was discarded and crystals were washed with methanol followed by diethyl ether and then dried. Yield: 0.033 g (72%, based on Co) M. p.: >250 °C. IR (KBr): υ/cm^{-1}= 3413 (br), 2926 (w), 2143 (s), 2118 (s), 1659 (s), 1550 (s), 1461 (w), 1434 (w), 1378 (m), 1269 (m), 1131 (m), 1051 (m), 893 (w), 811 (m), 741 (m), 540 (w). Elemental analysis: Found (calculated for $Co_2Fe_2K_2C_{42}H_{48}N_{22}O_{11}$): C, 37.88 (37.51); H, 3.60 (3.60); N, 22.92 (22.68). AAS Found (calculated for $Co_2Fe_2K_2C_{42}H_{48}N_{22}O_{11}$): Co, 8.52 (8.77); Fe, 8.09 (8.31); K, 5.61 (5.82).

Synthetic scheme of chiral ligands and precursor Cobalt complex:

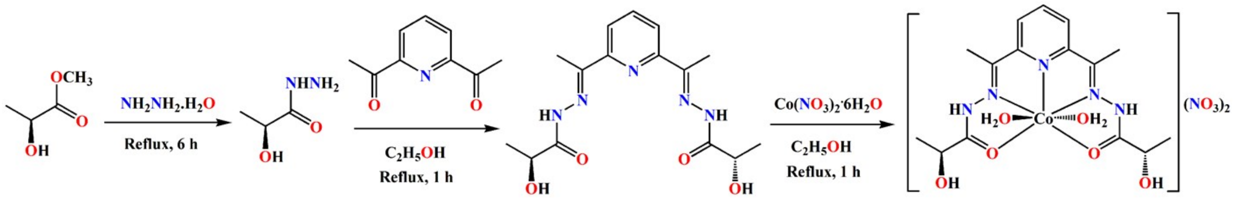

Scheme S1. Synthetic scheme of chiral hydrazide (*left*), chiral bis-hydrazone (*middle*) and 3*d* building block **1** (*right*).

NMR spectroscopy of (l)-2-hydroxypropanehydrazide:

The ^{1}H NMR spectrum of (*l*)-2-hydroxypropanehydrazide (Figure S1) shows a quartet peak at 3.9 ppm which is assigned to the -CH proton adjacent to the hydroxyl group. A doublet at 1.15 ppm corresponds to the methyl protons. A broad singlet at 8.8 ppm can be attributed to the –NH proton. The solvent residual peak for deuterated dimethyl sulfoxide arises at 2.4 ppm. The singlet peak at 3.1 ppm and 3.5 ppm are ascribed to the methyl protons of trace amount of methanol and water present, respectively, which are produced during the condensation reaction.[4] The ^{13}C-NMR spectrum of (*l*)-2-hydroxypropanehydrazide (Figure S2) displays a peak at 174.1 ppm which corresponds to the carbonyl carbon atom. The peak at 67.1 ppm can be ascribed to the CHOH carbon atom. The methyl carbon atom corresponds to the peak at 21.3 ppm. The peak at 49.1 ppm is assigned to the methyl carbon atom of methanol present in trace amount.

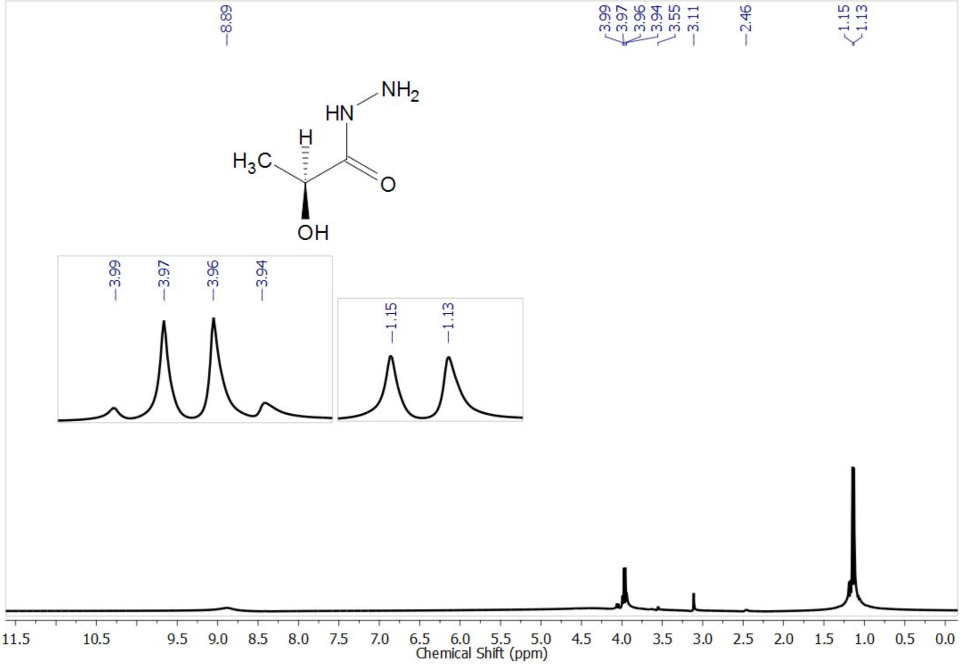

Figure S1. ^{1}H NMR spectrum of (*l*)-2-hydroxypropanehydrazide.

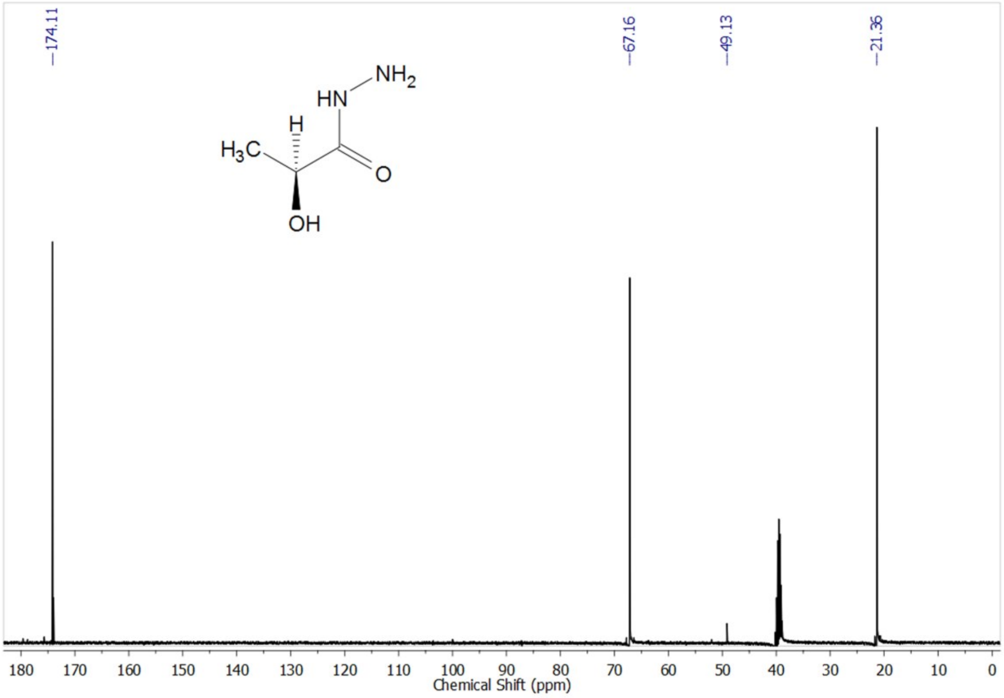

Figure S2. ^{13}C NMR spectrum of *(l)*-2-hydroxypropanehydrazide.

FT-IR spectra of l -2-hydroxypropane hydrazide and ***1****:*

The FT-IR spectrum of *(l)*-2-hydroxypropanehydrazide shows a broad peak at 3437 cm^{-1}which can be attributed to –NH stretching vibration (Figure S3). Intense peak observed at 1649 cm^{-1} can be assigned to the C=O stretching vibration of the hydrazide.

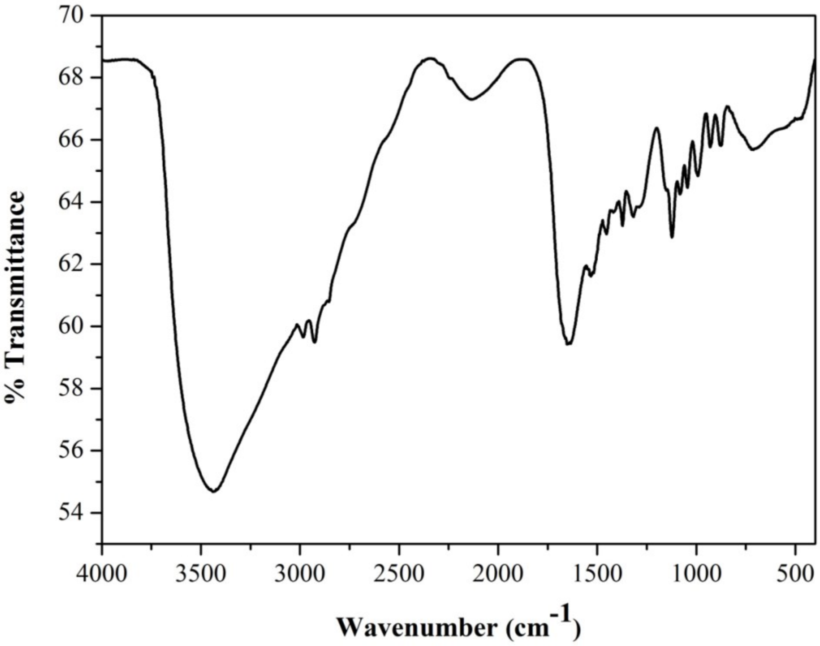

Figure S3. Infrared Spectrum of *(l)*-2-hydroxypropanehydrazide as KBr diluted discs.

Formation of the chiral bis-hydrazone ligand, *l*-daplh is confirmed by FT-IR spectroscopic technique (Figure S4). A characteristic broad peak at 3338 cm^{-1} corresponds to the –NH stretching frequency. Intense strong peak at 1668 cm^{-1} can be attributed to the C=N stretching vibration of the imine group.

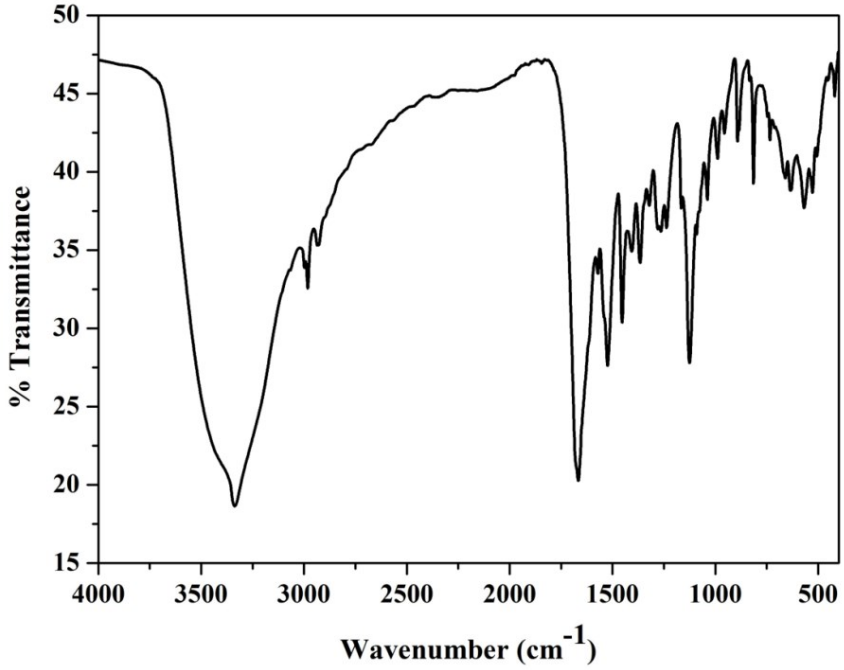

Figure S4. Infrared Spectrum of *l*-daplh as KBr diluted discs.

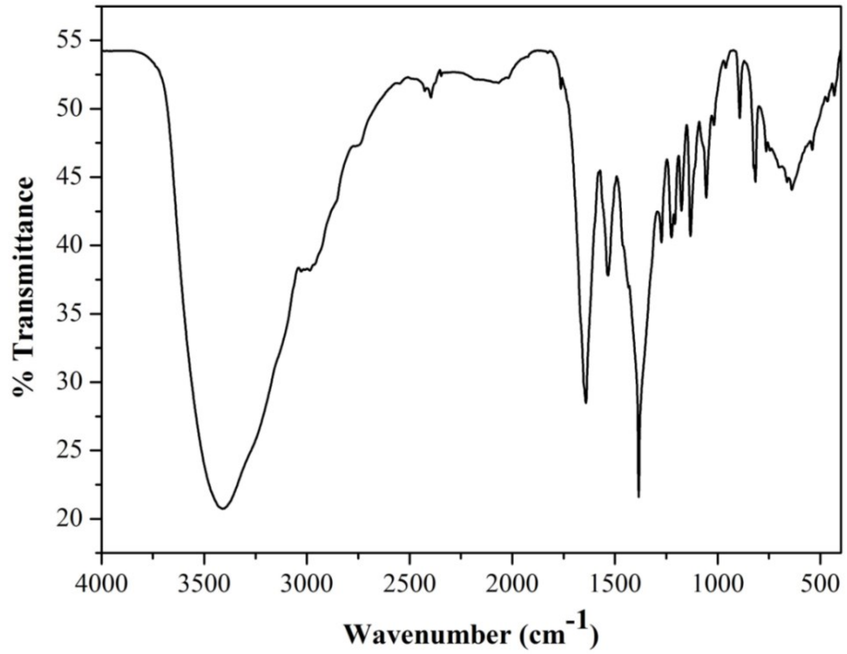

Figure S5. Infrared Spectrum of [Co(*l*-daplh)(H_2O)$_2$](NO_3)$_2$·2H_2O (**1**) as KBr diluted discs.

UV-visible spectra of chiral ligand *l*-daplh and [Co(*l*-daplh)$(H_2O)_2$]$(NO_3)_2$·$2H_2O$ **(1)** were measured in dimethyl sulfoxide solution (concentration: 1×10^{-5} mol L^{-1} at room temperature (Figure S6). The absorption band of the ligand located in the region of 270-340 nm can be primarily attributed to the π to π* electronic transition of *l*-daplh. As anticipated, the absorption profiles of complex [Co(*l*-daplh)$(H_2O)_2$]$(NO_3)_2$·$2H_2O$ are dominated by the ligand with the band slightly red shifted. The variations of the spectra imply that the chiral bis-hydrazone ligand *l*-daplh takes part in coordination with the complex [Co(*l*-daplh)$(H_2O)_2$]$(NO_3)_2$·$2H_2O$.

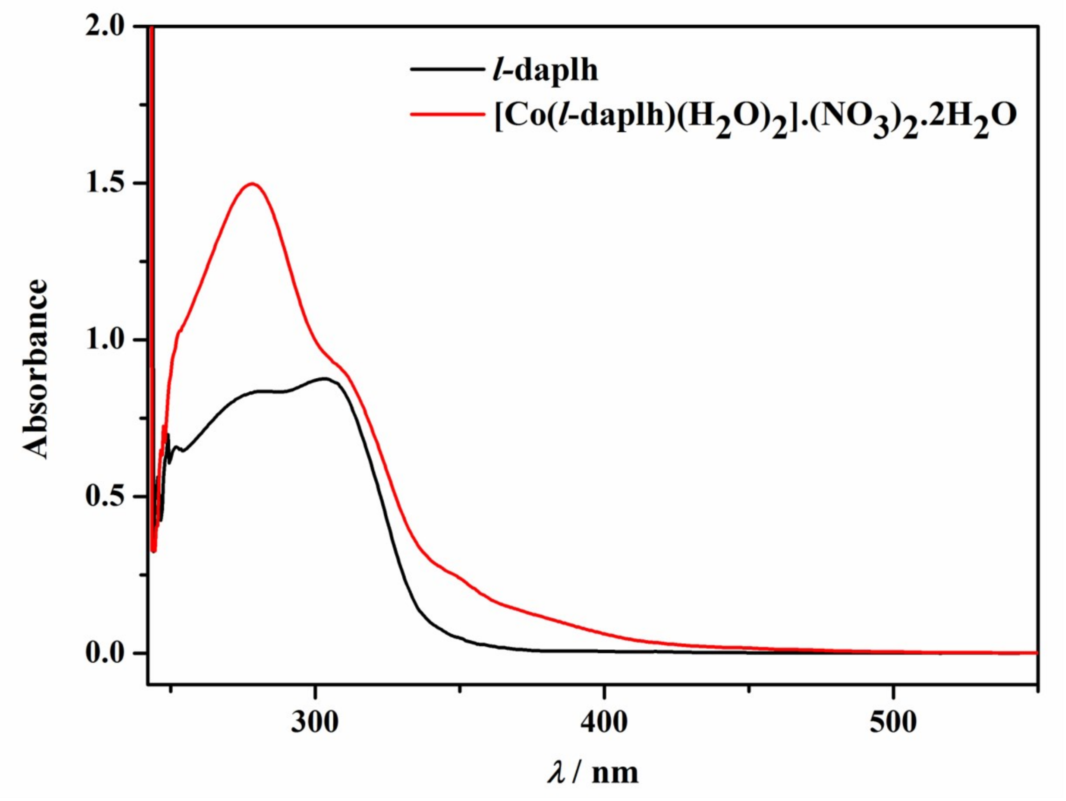

Figure S6. UV-visible spectra of *l*-daplh (*black line*) and [Co(*l*-daplh)$(H_2O)_2$]$(NO_3)_2$·$2H_2O$ **(1)** (*red line*), recorded in dimethyl sulfoxide at room temperature.

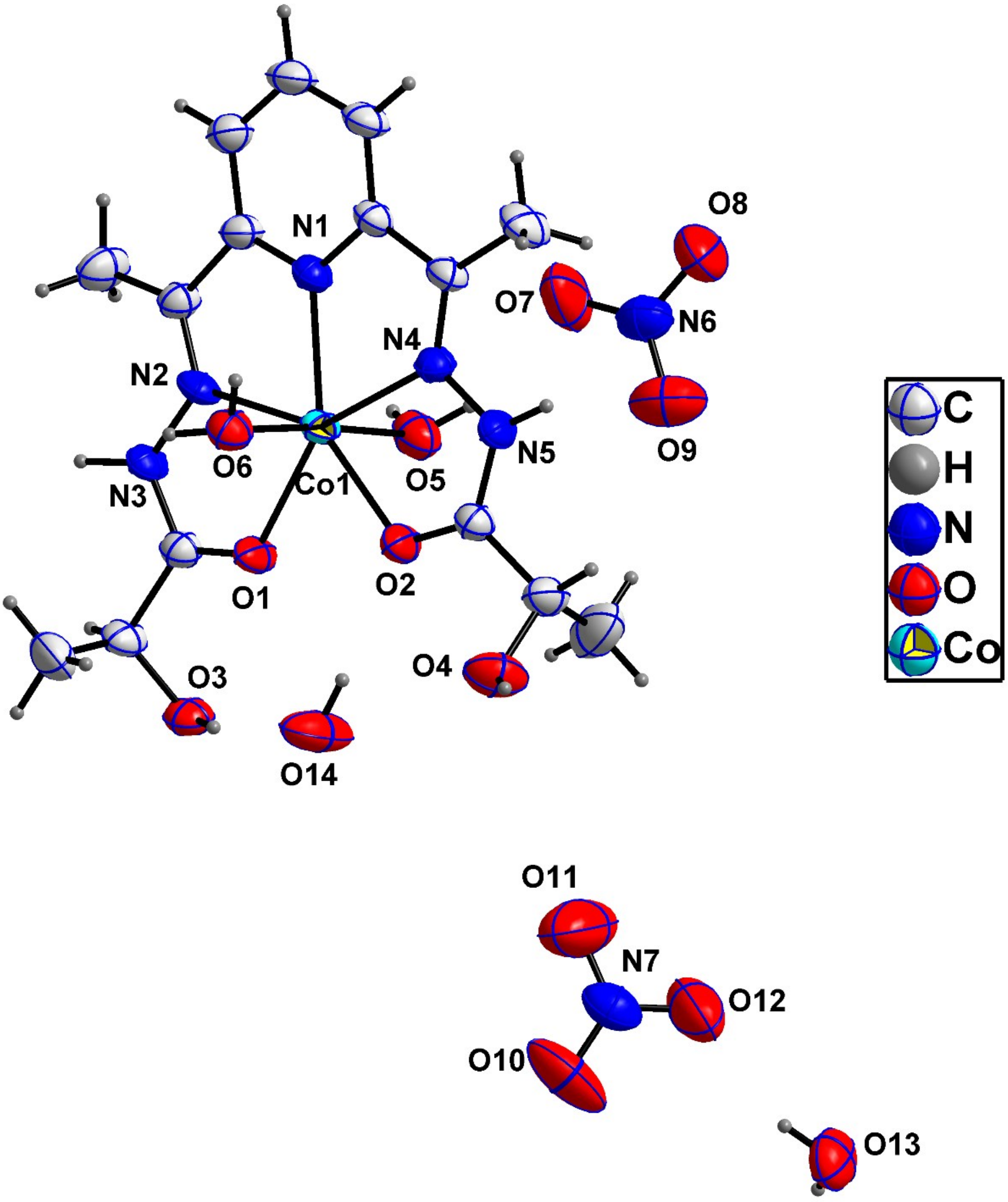

Figure S7. Thermal ellipsoid plot (50% probability) of molecular structure of **1.**

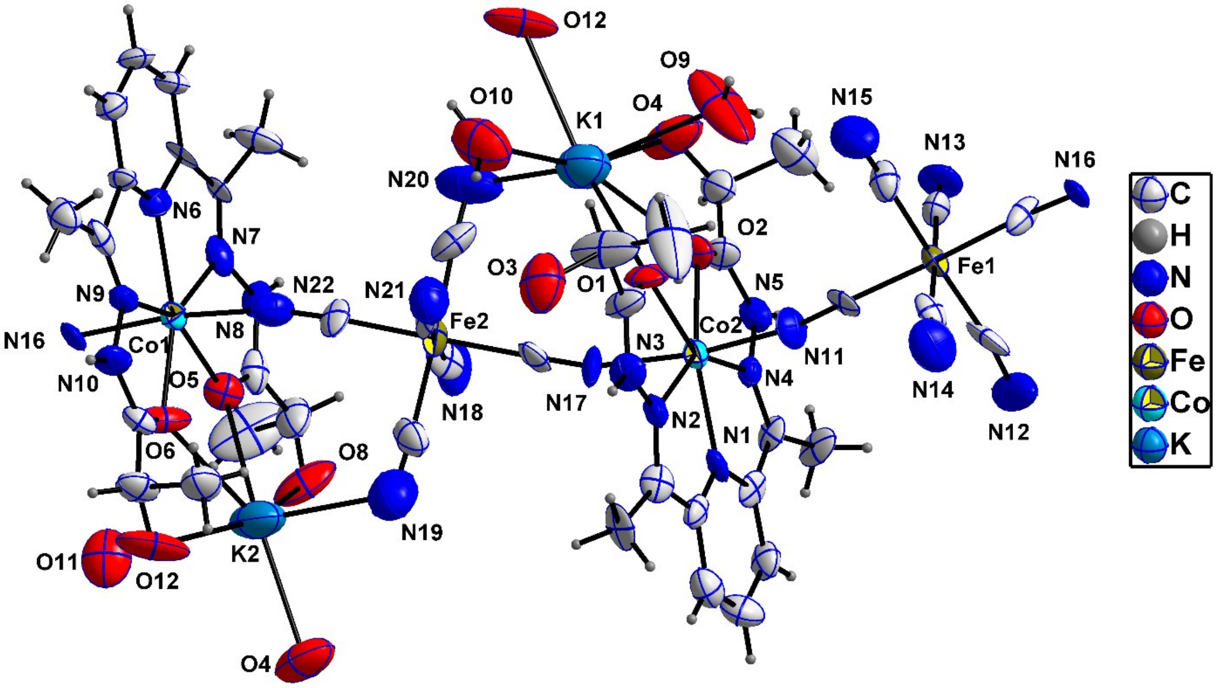

Figure S8. Thermal ellipsoid plot (50% probability) of asymmetric unit in **2**.

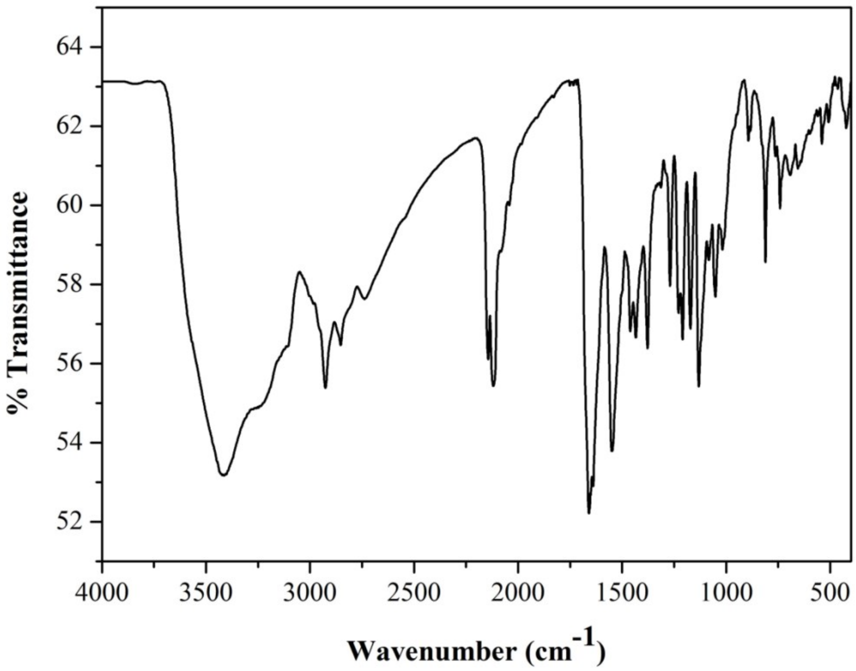

Figure S9. Infrared Spectrum of **2** as KBr diluted discs.

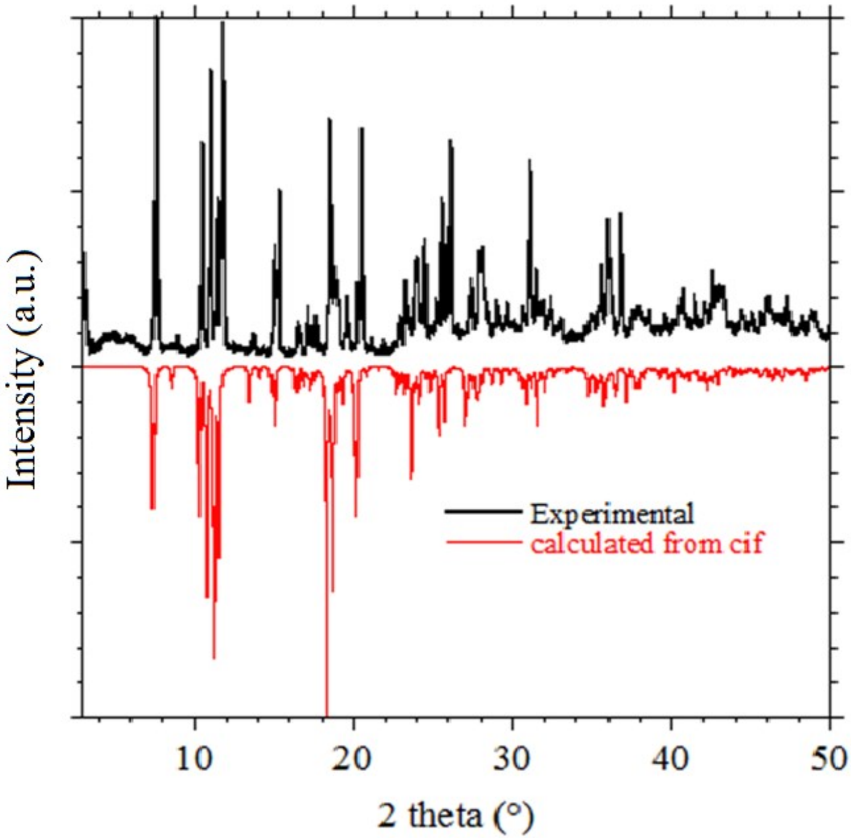

Figure S10. Powder X-ray diffraction pattern of **2**. Black line represents the experimental values and red line represents the calculated pattern.

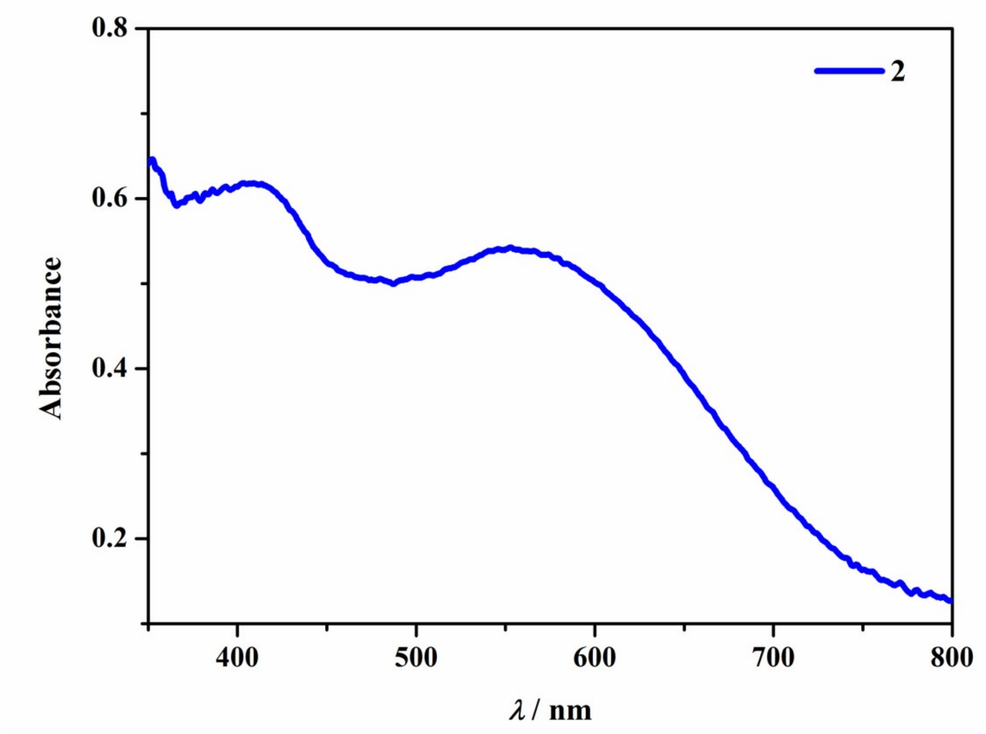

Figure S11. Solid-state UV-visible spectrum of **2**, recorded at 25º C.

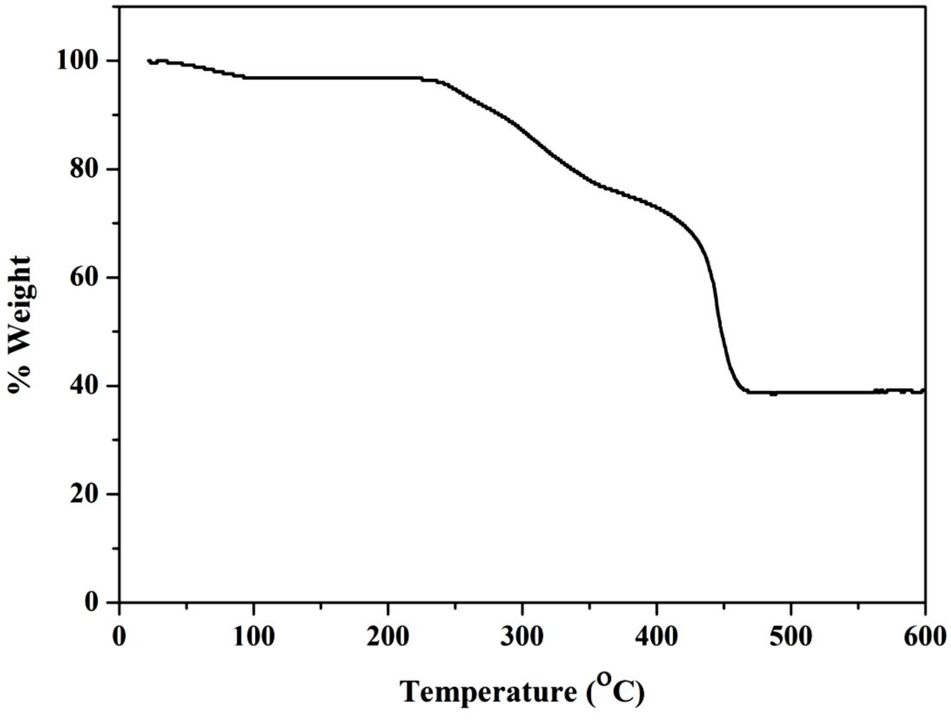

Figure S12. TGA pattern of **2**.

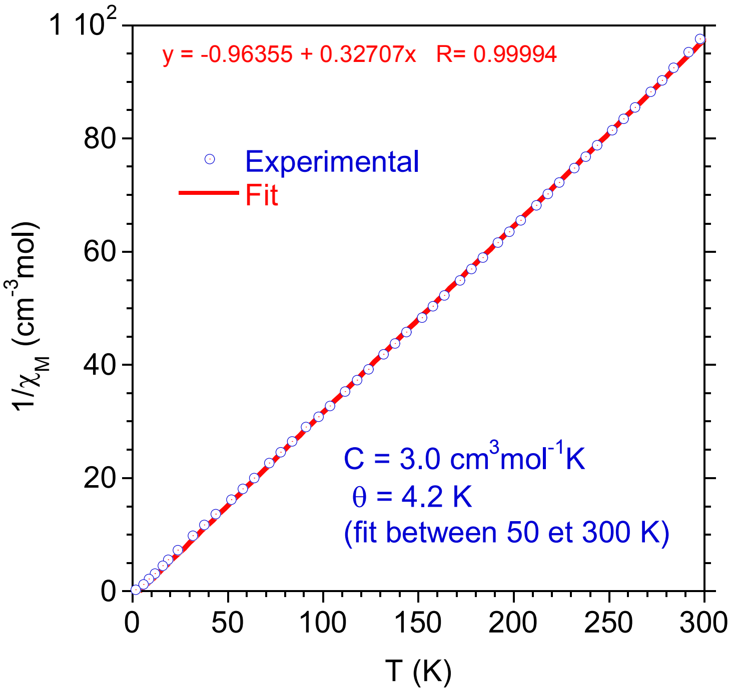

Figure S13. Variation of $1/\chi_M$ against temperature for **2**. Circles represent experimental value and the solid line represents the fit of a Curie-Weiss model.

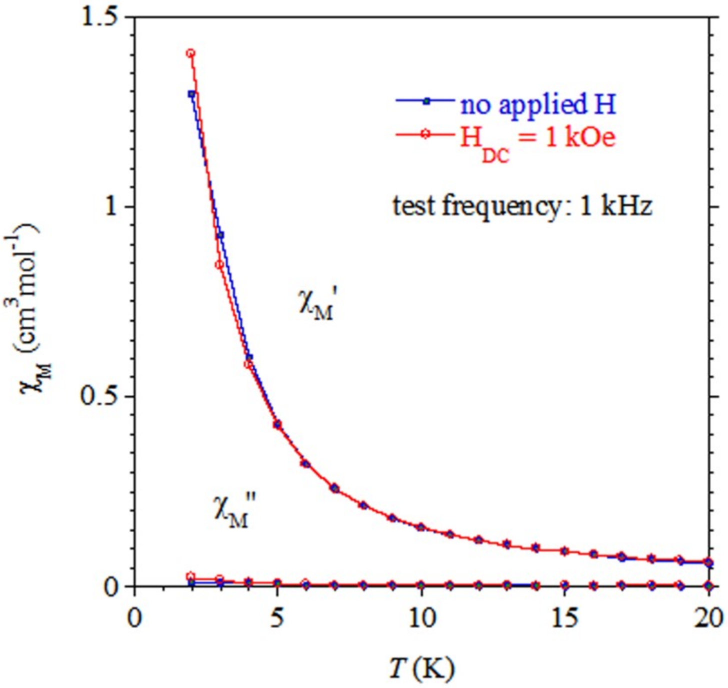

Figure S14. Temperature dependence of in-phase (χ_M') and out-of-phase (χ_M'') susceptibility under absence of applied field (*blue*) and 1 KOe applied field (*red*) for **2**.

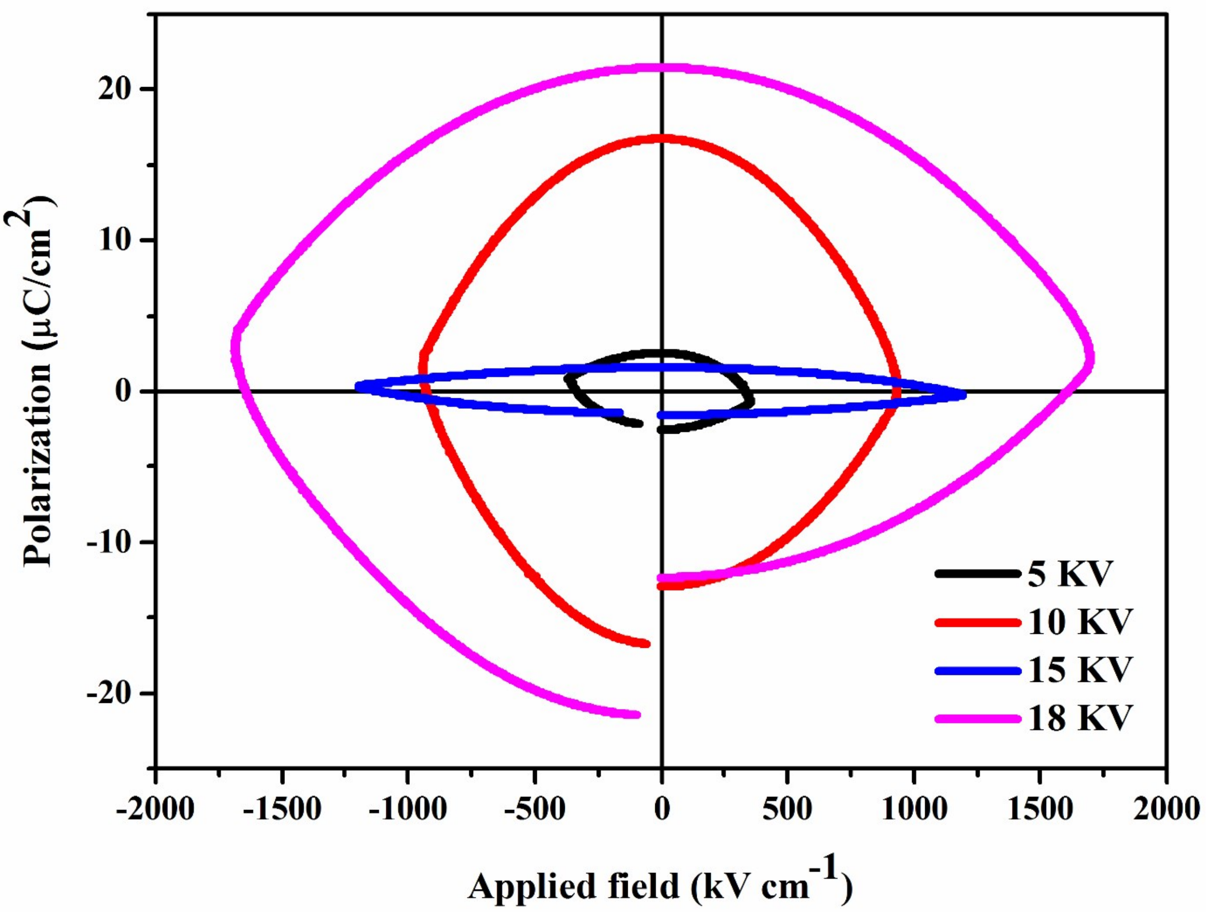

Figure S15. Polarization versus applied electric field of **1** at different applied voltages recorded at 20 °C.

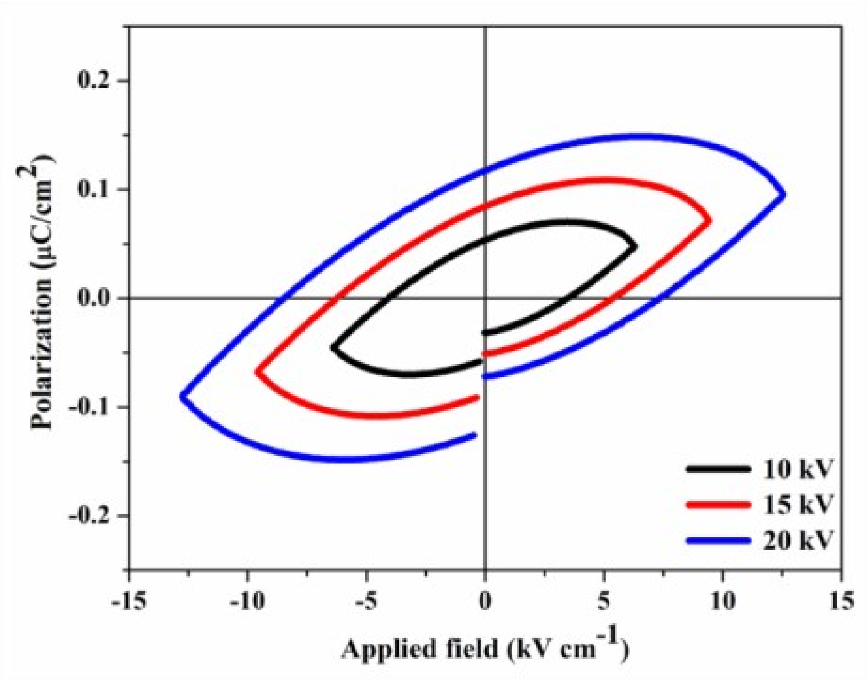

Figure S16. Polarization versus applied electric field (P-E hysteresis curves) of **2** at different applied voltages recorded at 20 °C.

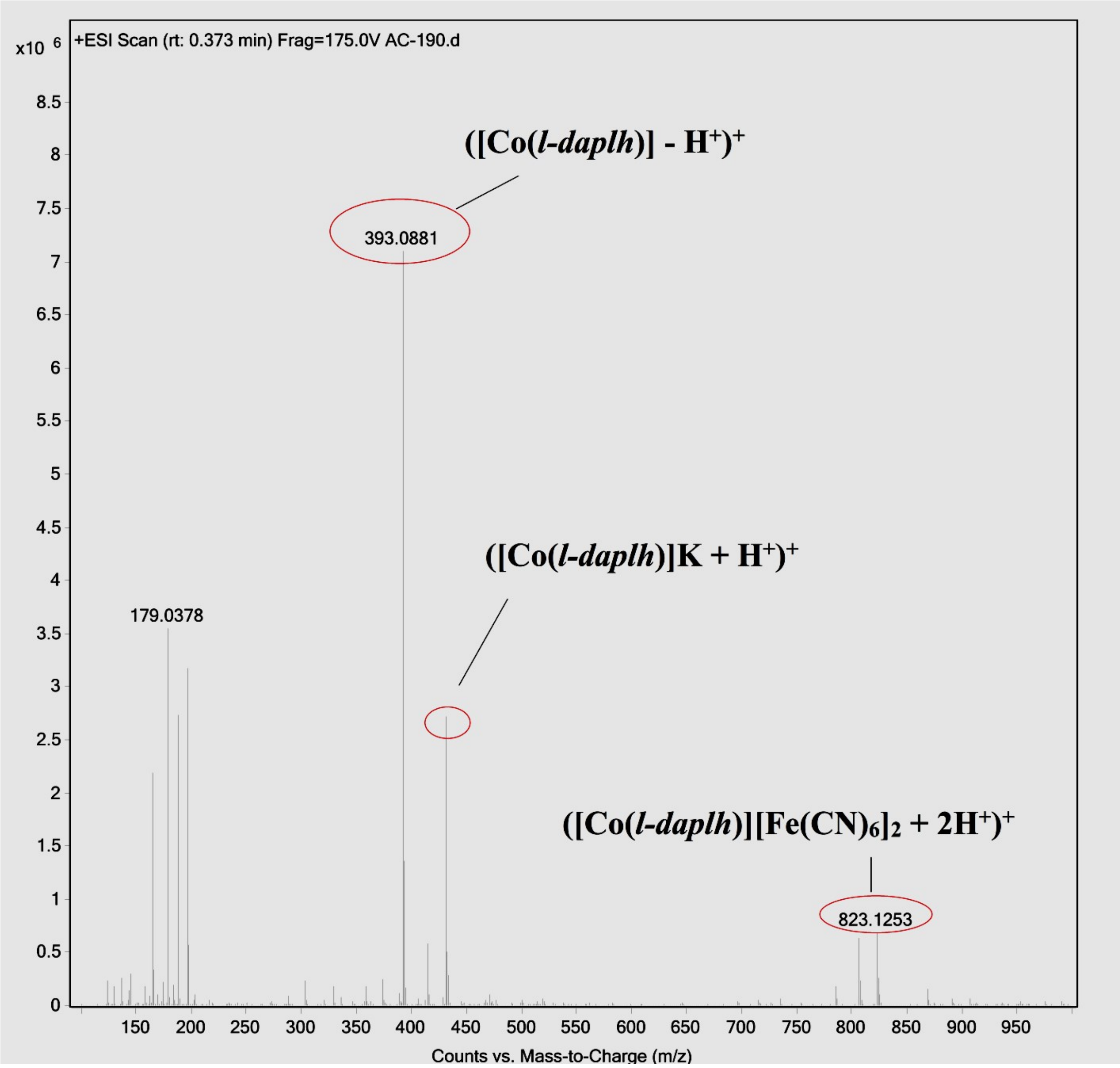

Figure S17. ESI- mass spectrum of **2**.

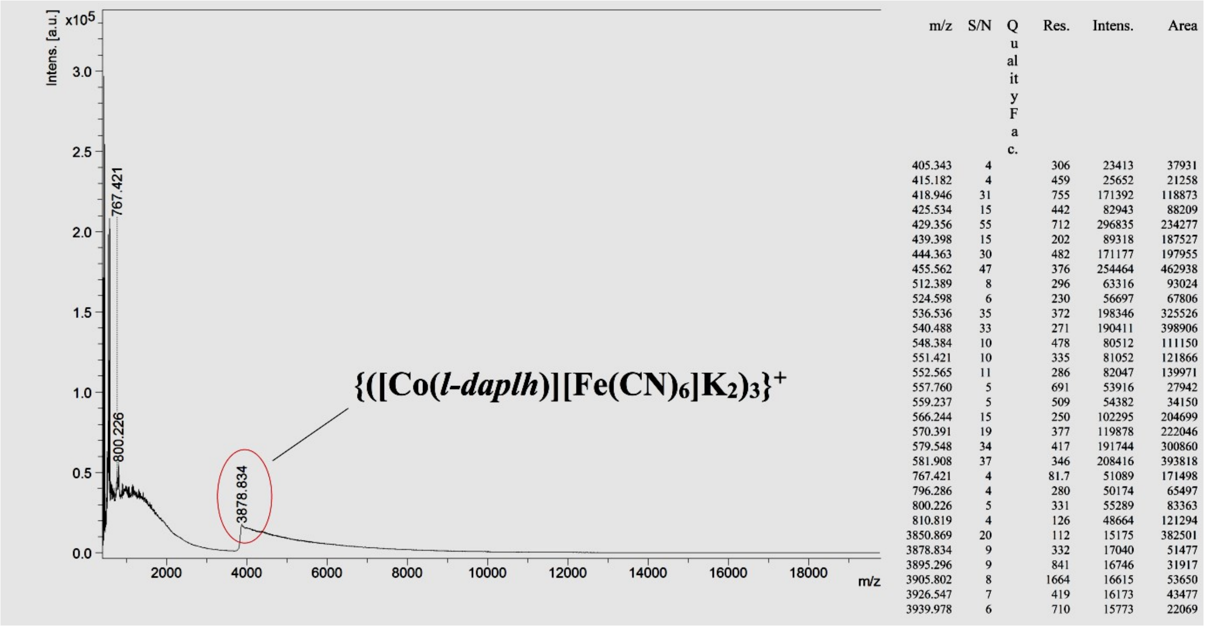

m/z	S/N	Quality Fac.	Res.	Intens.	Area
405.343	4		306	23413	37931
415.182	4		459	25652	21258
418.946	31		755	171392	118873
425.534	15		442	82943	88209
429.356	55		712	296835	234277
439.398	15		202	89318	187527
444.363	30		482	171177	197955
455.562	47		376	254464	462938
512.389	8		296	63316	93024
524.598	6		230	56697	67806
536.536	35		372	198346	325526
540.488	33		271	190411	398906
548.384	10		478	80512	111150
551.421	10		335	81052	121866
552.565	11		286	82047	139971
557.760	5		691	53916	27942
559.237	5		509	54382	34150
566.244	15		250	102295	204699
570.391	19		377	119878	222046
579.548	34		417	191744	300860
581.908	37		346	208416	393818
767.421	4		81.7	51089	171498
796.286	4		280	50174	65497
800.226	5		331	55289	83363
810.819	4		126	48664	121294
3850.869	20		112	15175	382501
3878.834	9		332	17040	51477
3895.296	9		841	16746	31917
3905.802	8		1664	16615	53650
3926.547	7		419	16173	43477
3939.978	6		710	15773	22069

Figure S18. MALDI-TOF mass spectrum of **2** in water.

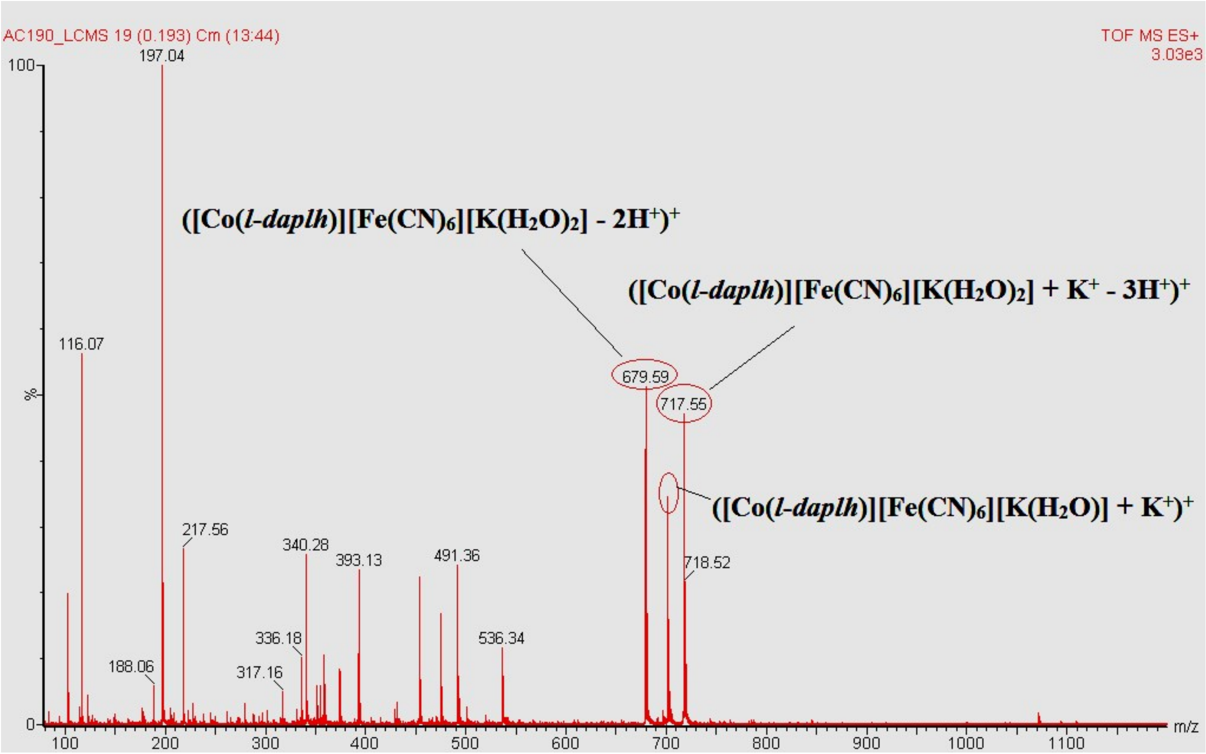

Figure S19. LC-mass spectrum of **2** in water.

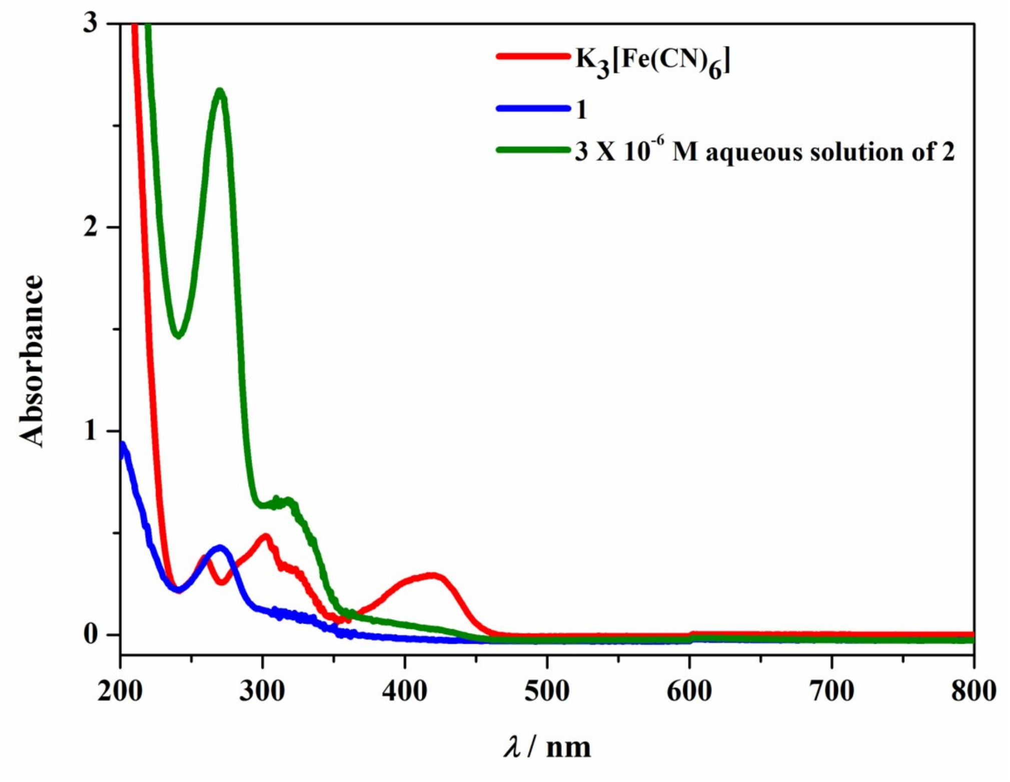

Figure S20. UV-visible spectra of **2** and individual building blocks in water recorded at room temperature.

Figure S21. Photograph of Tyndall effect in presence of LASER beam. Blank water in presence of LASER light (*left*), aqueous solution of **2** (*middle*) and aqueous solution of **2** in presence of LASER light (*right*).

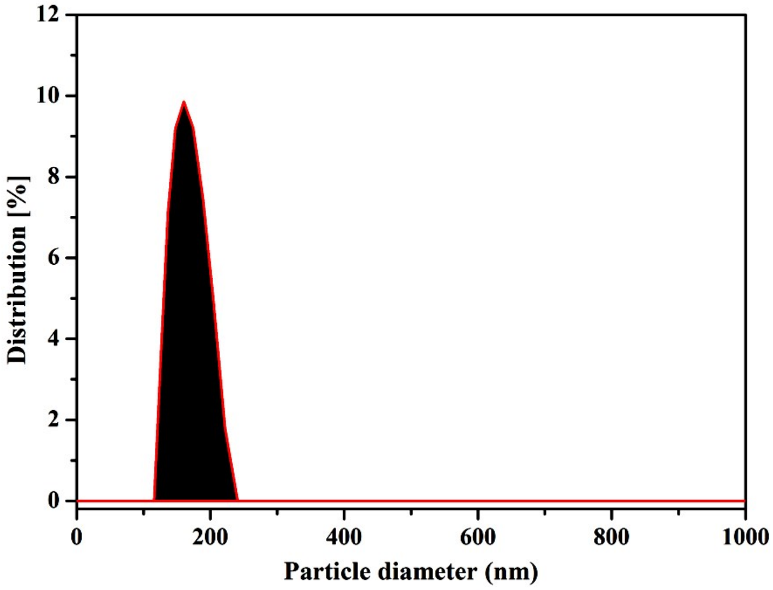

Figure S22. DLS spectrum of an aqueous solution of **2**.

Table S1. Crystal data and refinement parameters of **1** and **2**.

Complex	**1**	**2**
Empirical formula	$C_{15}H_{29}N_7O_{14}Co$	$C_{42}H_{48}Co_2Fe_2K_2N_{22}O_{11}$
Formula weight	590.38	1344.76
CCDC	1998743	1998744
Temperature/K	100	100
Crystal system	Monoclinic	Triclinic
Space group	$P\ 2_1$	P *1*
a/Å	8.182(3)	10.251(5)
b/Å	16.379(7)	11.759(5)
c/Å	9.224(4)	11.983(5)
α/°	90	92.379(5)
β/°	93.177(5)	91.977(5)
γ/°	90	91.531(5)
Volume/Å^3	1234.2(9)	1441.8(11)
Z	2	1
ρ_{calc}	1.589 mg/m^3	1.544 mg/m^3
μ/mm^{-1}	0.777	1.276
Crystal size, mm^3	0.16x0.15x0.12	0.16x0.15x0.12
F(000)	614	682
Theta range for data collection	2.211 to 26.998º	2.378 to 26.999º
Reflections collected/independent reflections	34374/5388	30004/12465
Completeness to theta	100%	99.9%
Absorption correction	Multi-scan	Multi-scan
Data / restraints / parameters	5388 / 14 / 383	12465 /3 / 739
Goodness-of-fit on F^2	1.160	1.287
Absolute structure parameter	0.021(11)	0.03(3)
Largest diff. peak and hole	0.683 and -0.353 e.Å^{-3}	1.540 and -0.980 e.Å^{-3}
Final R indexes [I>=2σ (I)]	R1 = 0.0461, wR2 = 0.0904	R1 = 0.0908, wR2 = 0.1838
Final R indexes [all data]	R1 = 0.0684, wR2 = 0.0981	R1 = 0.1552, wR2 = 0.2102

Table S2. Selected bond lengths [Å] and bond angles [°] of **1**

Bonds lengths	**1**	**Bond Angles**	**1**
Co(1)-N(1)	2.152(4)	O(1)-Co(1)-N(2)	71.27(14)
Co(1)-N(2)	2.188(5)	N(2)-Co(1)-N(1)	70.64(16)
Co(1)-N(4)	2.171(4)	N(1)-Co(1)-N(4)	71.15(17)
Co(1)-O(1)	2.144(4)	N(4)-Co(1)-O(2)	71.93(15)
Co(1)-O(2)	2.189(4))	O(2)-Co(1)-O(1)	75.10(14)
Co(1)-O(5)	2.164(5)	N(1)-Co(1)-O(5)	91.82(18)
Co(1)-O(6)	2.142(4)	N(1)-Co(1)-O(6)	92.42(17)
		O(5)-Co(1)-O(6)	175.4(2)

Table S3. Shape analysis data of **1** and **2**.

Complex	**PBPY-7**	**JPBPY-7**
1(Co)	**0.102**	3.584
2(Co1)	**0.310**	2.973
2(Co2)	**0.338**	3.165

PBPY-7: Pentagonal bipyramid (D_{5h}); JPBPY-7: Johnson pentagonal bipyramid J13 (D_{5h})

Table S4. Selected bond lengths [Å] and bond angles [°] of **2**

Co(1)-N(6)	2.166(16)	N(16)-C(32)- Fe(1)	175(2)
Co(1)-N(7)	2.256(19)	N(11)-Co(2)-N(17)	172.3(7)
Co(1)-N(9)	2.197(18)	N(1)-Co(2)-O(1)	142.0(7)
Co(1)-N(22)	2.037(19)	N(1)-Co(2)-O(2)	141.3(6)
Co(1)-N(16)	2.119(18)	N(2)-Co(2)-O(1)	71.0(6)
Co(1)-O(5)	2.188(15)	N(4)-Co(2)-O(1)	147.6(7)
Co(1)-O(6)	2.208(16)	N(2)-Co(2)-O(2)	146.6(6)
Co(2)-N(11)	2.054(18)	N(4)-Co(2)-O(2)	71.5(6)
Co(2)-N(17)	2.126(17)	O(1)-Co(2)-O(2)	76.4(6)
Co(2)-N(1)	2.143(17)	O(5)-Co(1)-O(6)	76.7(6)
Co(2)-N(2)	2.156(18)	Co(1)-O(5)-K(2)	112.2(6)
Co(2)-N(4)	2.188(16)	Co(1)-O(6)-K(2)	109.0(7)
Co(2)-O(1)	2.216(15)	O(5)-K(2)-O(6)	58.0(5)
Co(2)-O(2)	2.207(15)	O(11)-K(2)-N(19)#3	146.0(7)
K(1)-O(1)	2.871(18)	O(5)-K(2)-N(19)#3	108.9(7)
K(1)- O(2)	2.825(16)	O(5)-K(2)-O(8)	56.7(4)
K(1)- O(4)	3.028(19)	O(5)-K(2)-O(4)#2	162.8(6)
K(1)- O(9)	2.87(2)	O(5)-K(2)-O(11)	87.8(5)
K(1)-O(10)	2.656(17)	O(6)-K(2)-O(11)	65.4(5)
K(1)-O(12)#2	3.000(19)	O(4)#2-K(2)-O(6)	138.1(6)
K(1)-N(20)	2.87(3)	O(6)-K(2)-O(8)	114.5(5)
K(2)- O(5)	2.776(16)	Co(2)-O(1)-K(1)	106.4(7)
K(2)- O(6)	2.849(19)	Co(2)-O(2)-K(1)	108.2(5)
K(2)- O(8)	2.722(16)	O(1)-K(1)-O(2)	57.4(5)
K(2)-O(4)#2	2.811(17)	N(20)-K(1)-O(9)	147.5(9)
K(2)-O(11)	2.927(18)	O(1)-K(1)-N(20)	126.5(7)
K(2)-O(12)	3.07(2)	O(1)-K(1)-O(10)	91.7(6)
K(2)-N(19)#1	3.25(3)	O(1)-K(1)-O(12)#4	157.1(5)
N(6)-Co(1)-O(5)	141.4(6)	O(1)-K(1)-O(9)	78.1(8)
N(6)-Co(1)-O(6)	141.7(7)	O(1)-K(1)-O(4)	110.7(5)
N(9)-Co(1)-O(5)	147.1(6)	O(2)-K(1)-O(4)	54.5(4)
N(6)-Co(1)-N(9)	71.2(6)	O(2)-K(1)-O(9)	66.5(5)
N(7)-Co(1)-O(5)	70.5(6)	O(9)-K(1)-O(10)	117.0(6)
N(22)-Co(1)-N(16)	172.7(7)		

Symmetry transformations used to generate equivalent atoms: #1 x+1,y+1,z-1 #2 x-1,y-1,z #3 x-1,y-1,z+1 #4 x+1,y+1,z

References:

(1) G. M. Sheldrick, *Acta Crystallographica Section A: Foundations of Crystallography*, 2008, **64**, 112.

(2) R. Georges, J. J. Borras-Almenar, E. Coronado, J. Curély, M. Drillon, In *Magnetism: Molecules to materials: Models and experiments*; J. S. Miller and M. Drillon, Ed.; Wiley-VCH: Weinheim, 2002; Vol. 1, p 15

(3) N. Noshiranzadeh, A. Heidari, F. Haghi, R. Bikas and T. Lis, *J. Mol. Str.,* 2017, **1128**, 391.

(4) G. R. Fulmer, A. J. Miller, N. H. Sherden, H. E. Gottlieb, A. Nudelman, B. M. Stoltz, J. E. Bercaw and K. I. Goldberg, *Organometallics,* 2010, **29**, 2176.